Electronic Supplementary Material (ESI) for Nanoscale.

Hollow Porous Cu Particles from Silica-encapsulated Cu_2O Nanoparticle Aggregates Effectively Catalyze 4-nitrophenol Reduction

Jianwei Jiang,[†] Young Soo Lim,[‡] Sanghyuk Park,[§] Sang-Ho Kim,[§] Sungho Yoon[†,*], and Longhai Piao[§,*]

Supporting Information

List of Supporting Information

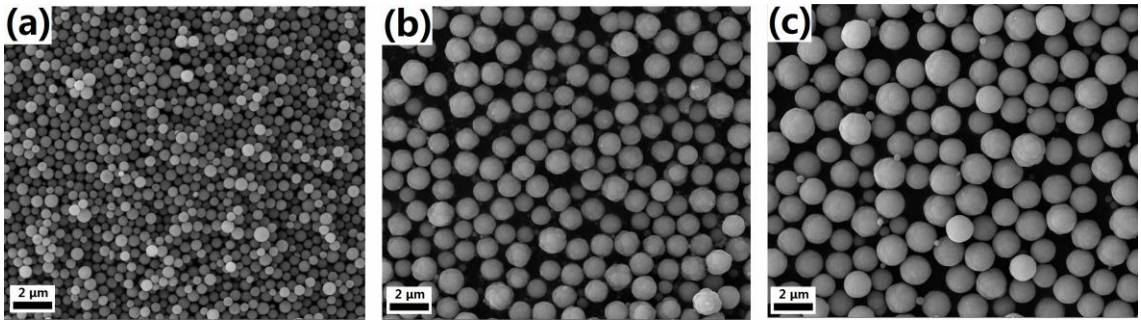

Figure S1 Control of the size of Cu_2O NPAs by varying the PVP-29,000 concentration: (a) 60 g/L (~500 nm), (b) 40 g/L (~930 nm), and (c) 20 g/L (~1.5 μm).

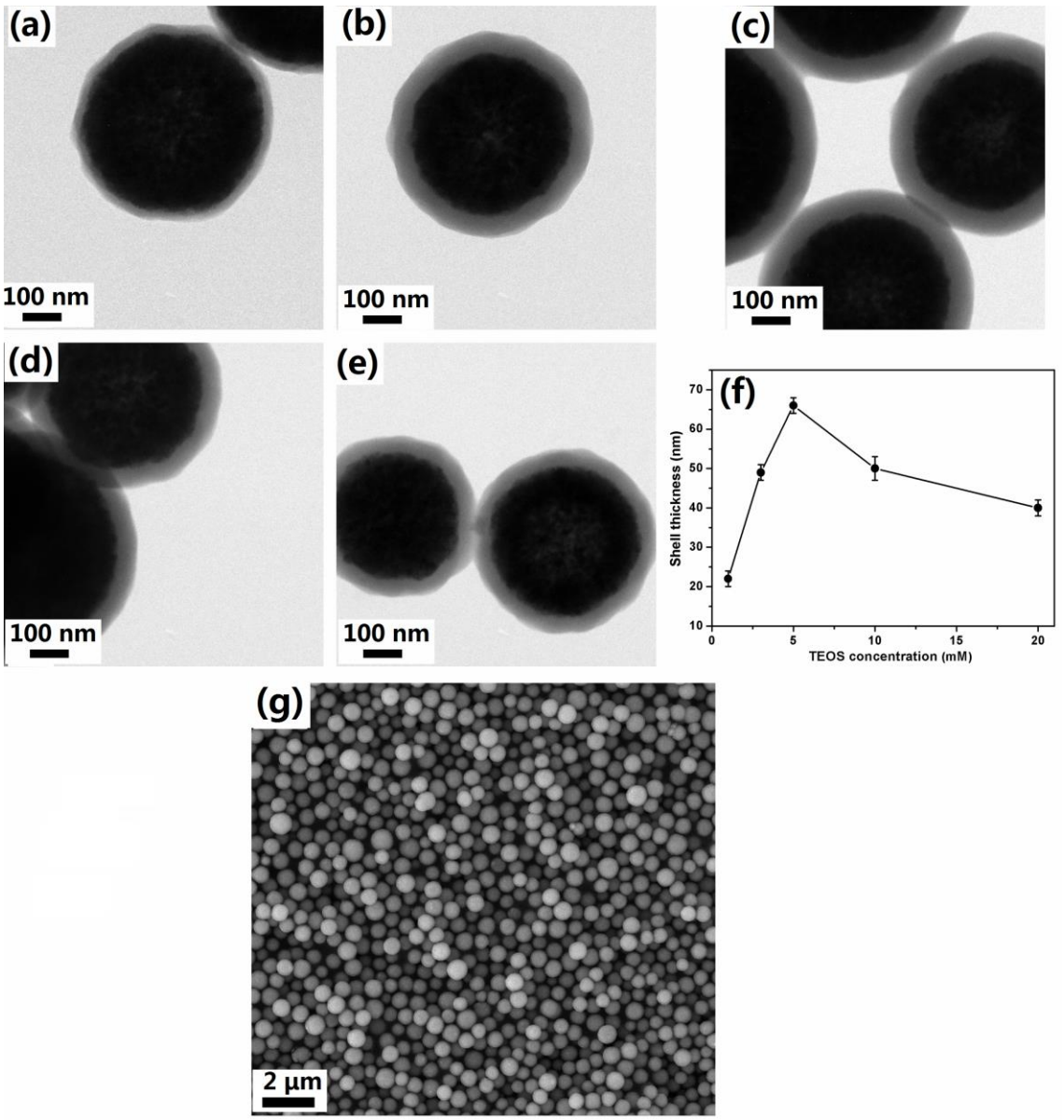

Figure S2 TEM images of the encapsulated Cu_2O NPAs (500 nm) with different TEOS concentrations: (a) 1.0 mM, (b) 3.0 mM, (c) 5.0 mM, (d) 10.0 mM, and (e) 20.0 mM. The concentrations of Cu_2O NPAs, H_2O, and NaOH were 0.5 g/L, 18 wt%, and 1.0 mM, respectively. (f) Shell thickness as a function of the TEOS concentration. (h) SEM image of silica-encapsulated Cu_2O NPAs at a TEOS concentration of 5.0 mM.

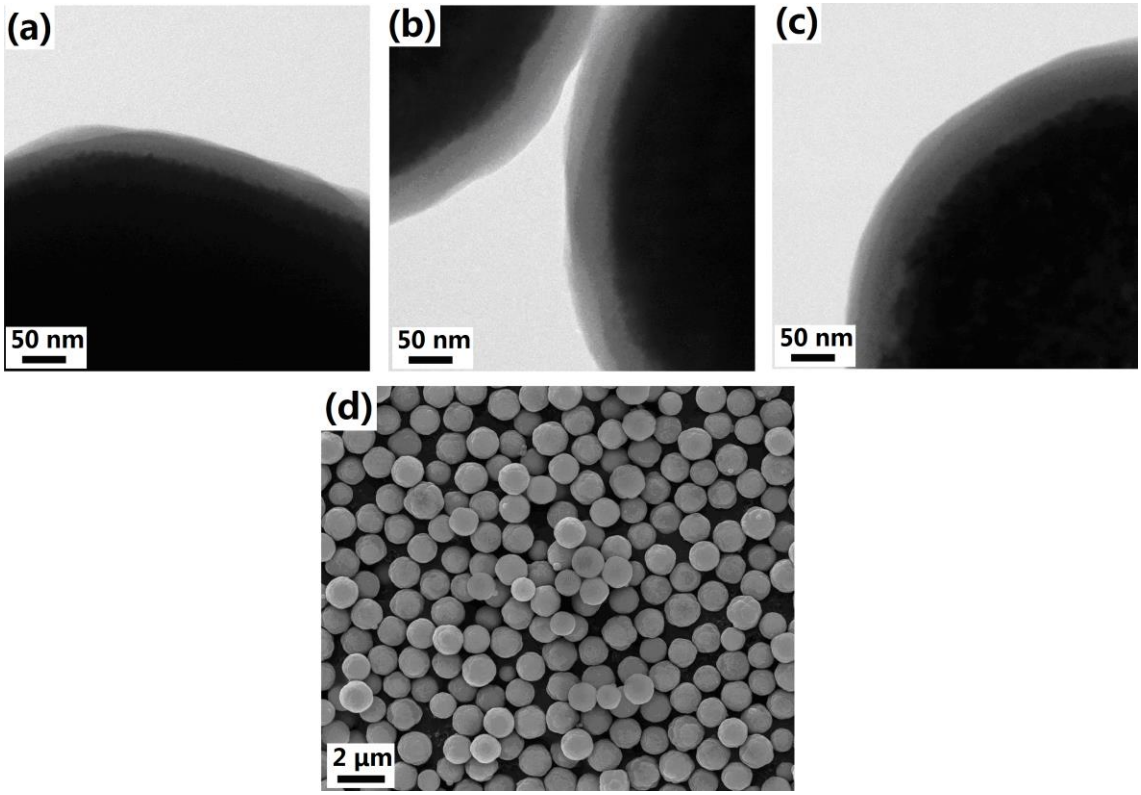

Figure S3 TEM images of the encapsulated Cu_2O NPAs (930 nm) with different TEOS concentrations: (a) 1.0 mM (28 nm), (b) 3.0 mM (45 nm), and (c) 5.0 mM (60 nm). The concentrations of Cu_2O NPAs, H_2O, and NaOH were 1.0 g/L, 18 wt%, and 1.0 mM, respectively. (d) SEM image of silica-encapsulated Cu_2O NPAs at a TEOS concentration of 5.0 mM.

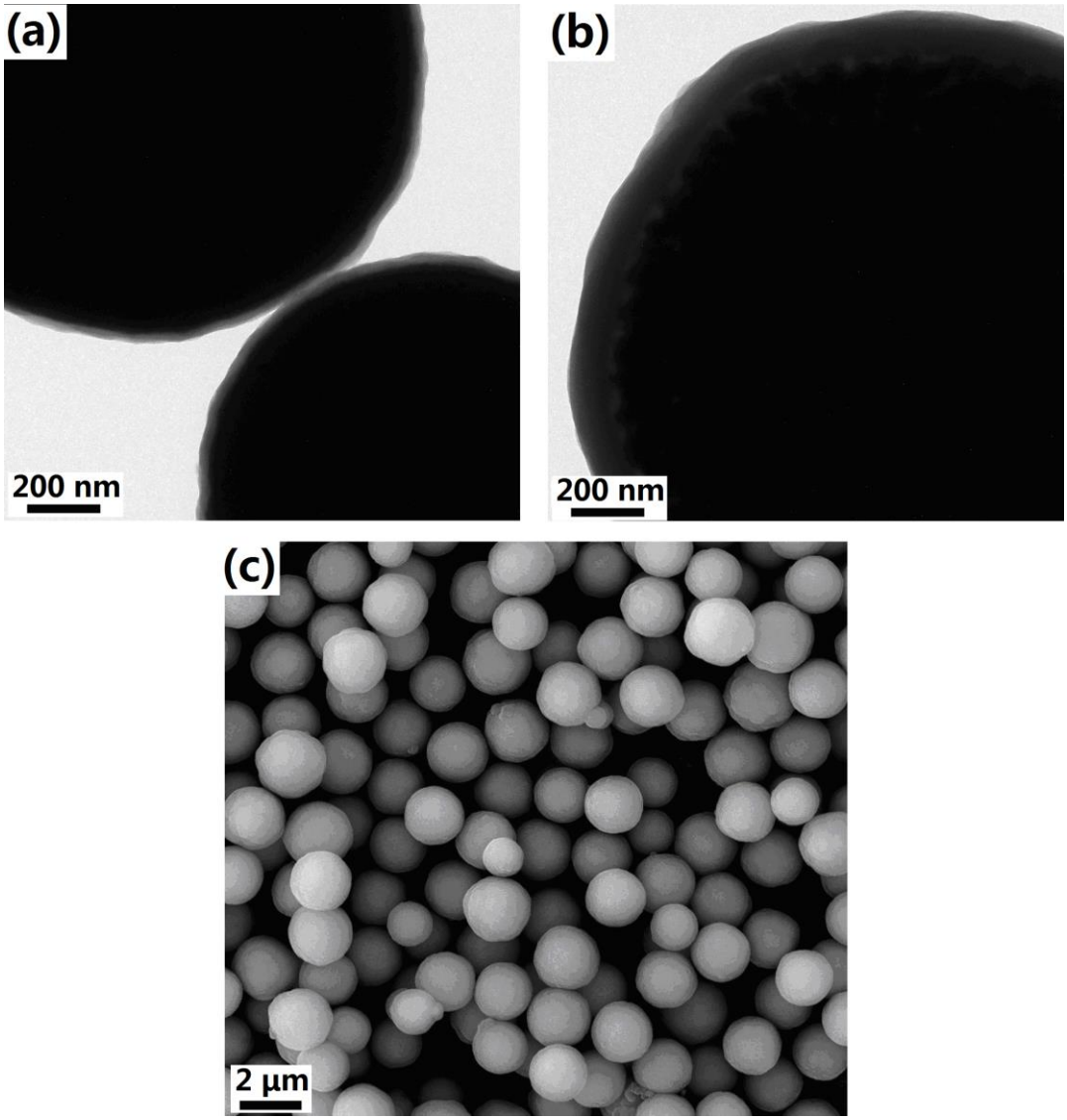

Figure S4 TEM images of the encapsulated Cu_2O NPAs (1.5 µm) after two encapsulations: (a) first encapsulation, TEOS concentration of 10.0 mM (shell thickness: 24 nm), and (b) second encapsulation, TEOS concentration of 10.0 mM (shell thickness: 88 nm). The concentrations of Cu_2O, H_2O, and NaOH were 1.0 g/L, 18 wt%, and 1.0 mM, respectively. SEM image of silica-encapsulated Cu_2O NPAs after two encapsulations.

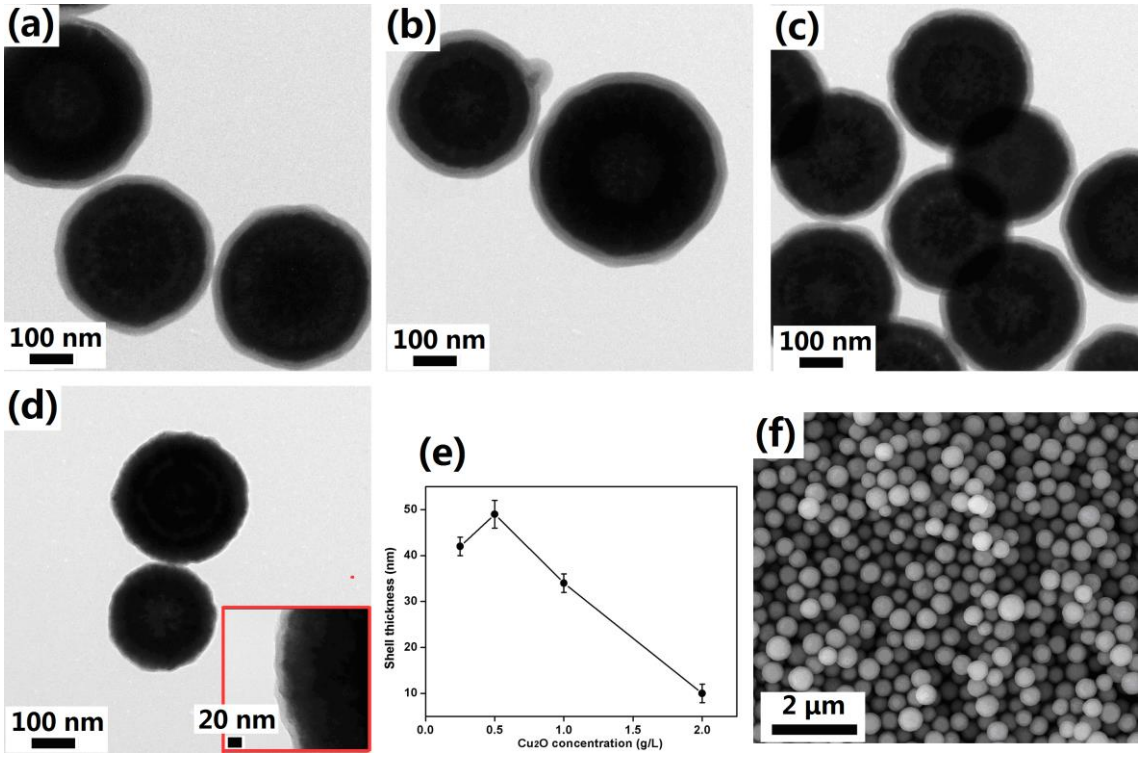

Figure S5 TEM images of the encapsulated Cu_2O NPAs (500 nm) with different Cu_2O concentrations: (a) 0.25 g/L, (b) 0.5 g/L, (c) 1.0 g/L, and (d) 2.0 g/L. The concentrations of TEOS, H_2O, and NaOH were 3.0 mM, 18 wt%, and 1.0 mM, respectively. (e) Shell thickness as a function of Cu_2O concentration. (f) SEM image of silica-encapsulated Cu_2O NPAs at a TEOS concentration of 5.0 mM.

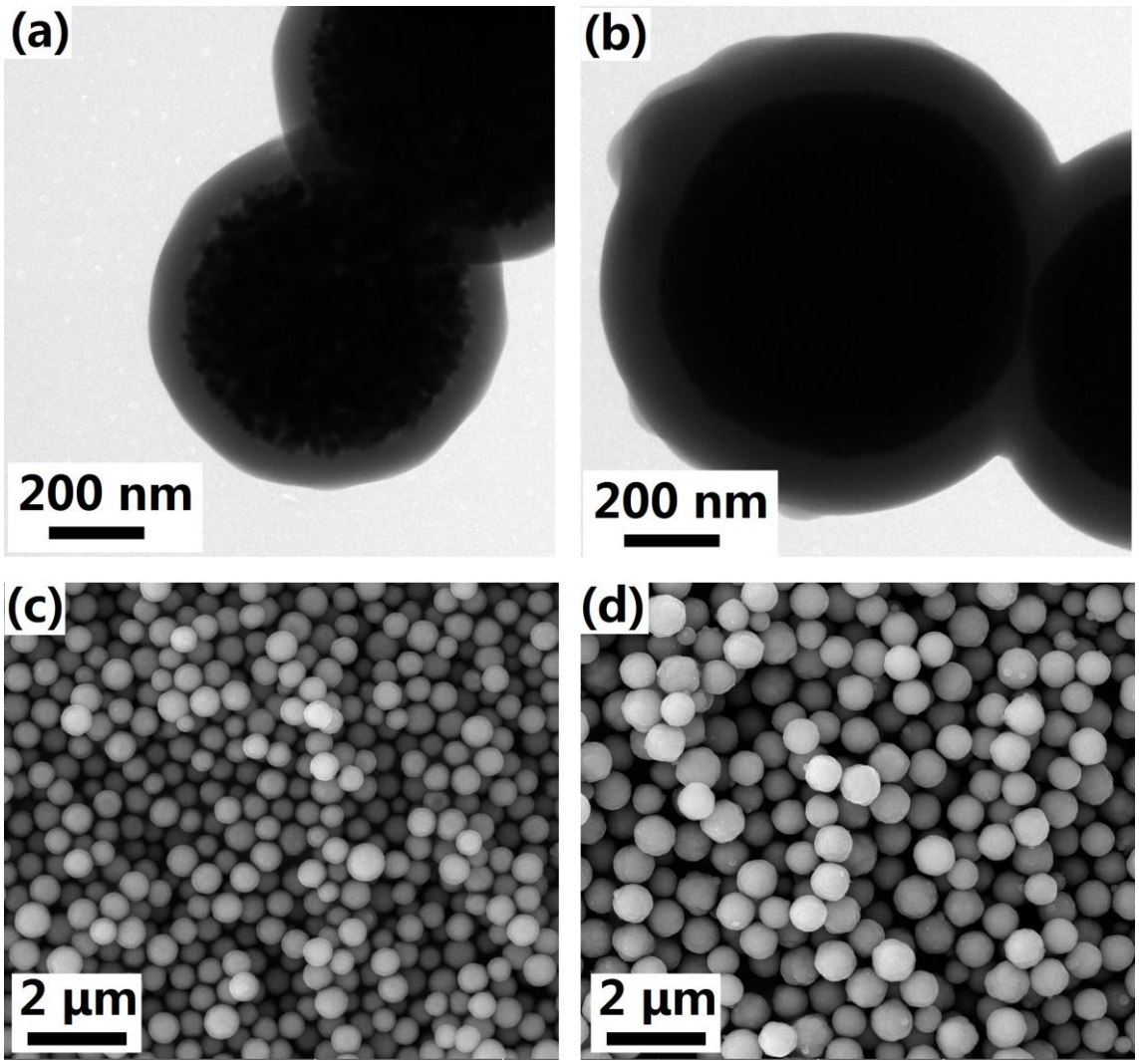

Figure S6 TEM images of the encapsulated Cu_2O NPAs after two encapsulations. (a) 500 nm (shell thickness: 100 nm) and (b) 930 nm (shell thickness: 120 nm. (c, d) Relevant SEM images. TEOS concentrations for the first and second encapsulations were 3.0 mM and 5.0 mM, respectively. The concentrations of Cu_2O, H_2O, and NaOH were 1.0 g/L, 18 wt%, and 1.0 mM, respectively.

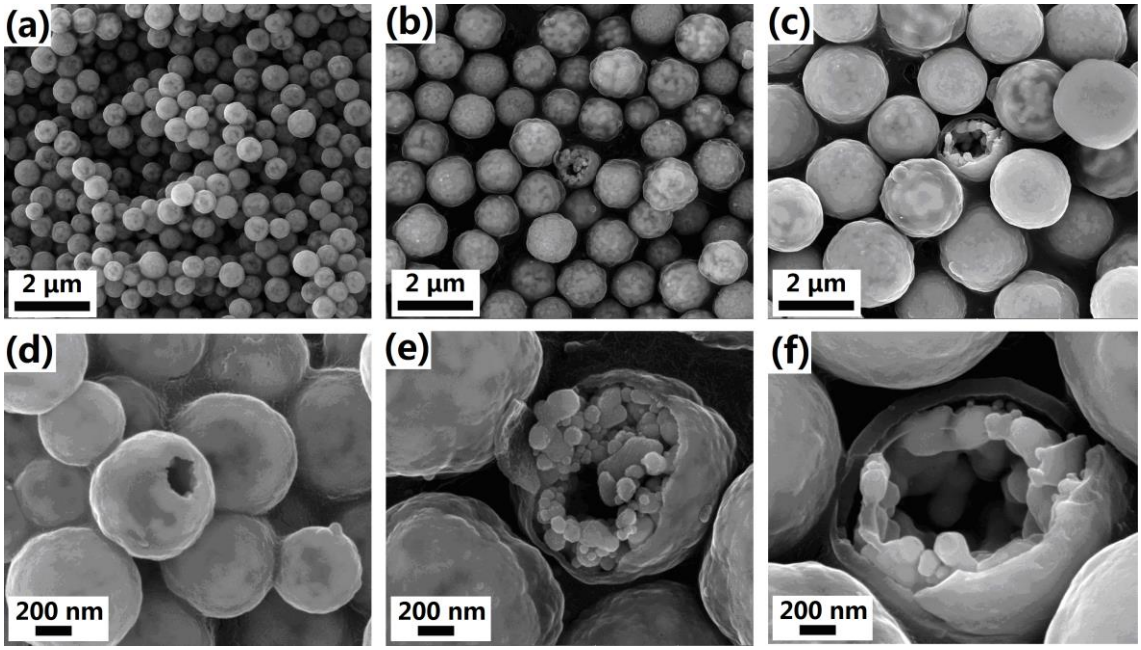

Figure S7 SEM images of particles from the PEG-400 reduction of $Cu_2O@SiO_2$ at 240 °C. (a) and (d) 500 nm particles with a shell thickness of 34 nm, (b) and (e) 930 nm particles with a shell thickness of 45 nm, and (c) and (f) 1.5 µm particles with a shell thickness of 88 nm.

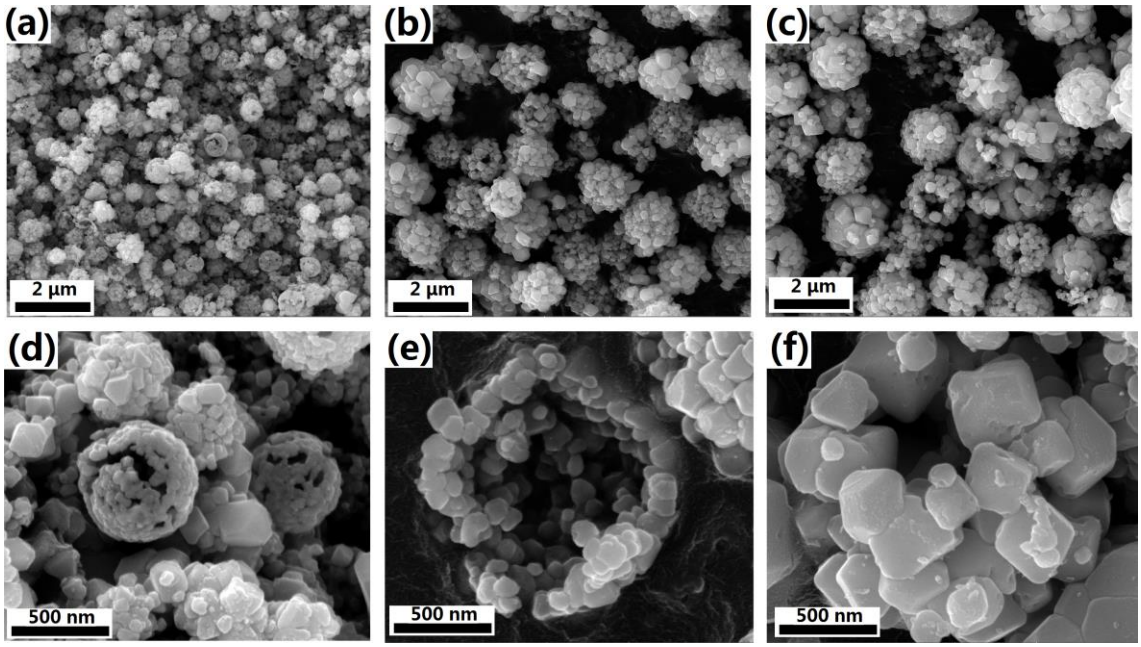

Figure S8 SEM images of particles from the removal of the silica shell using NaOH solution (a) and (d) 500 nm particles, (b) and (e) 930 nm particles, and (c) and (f) 1.5 µm particles

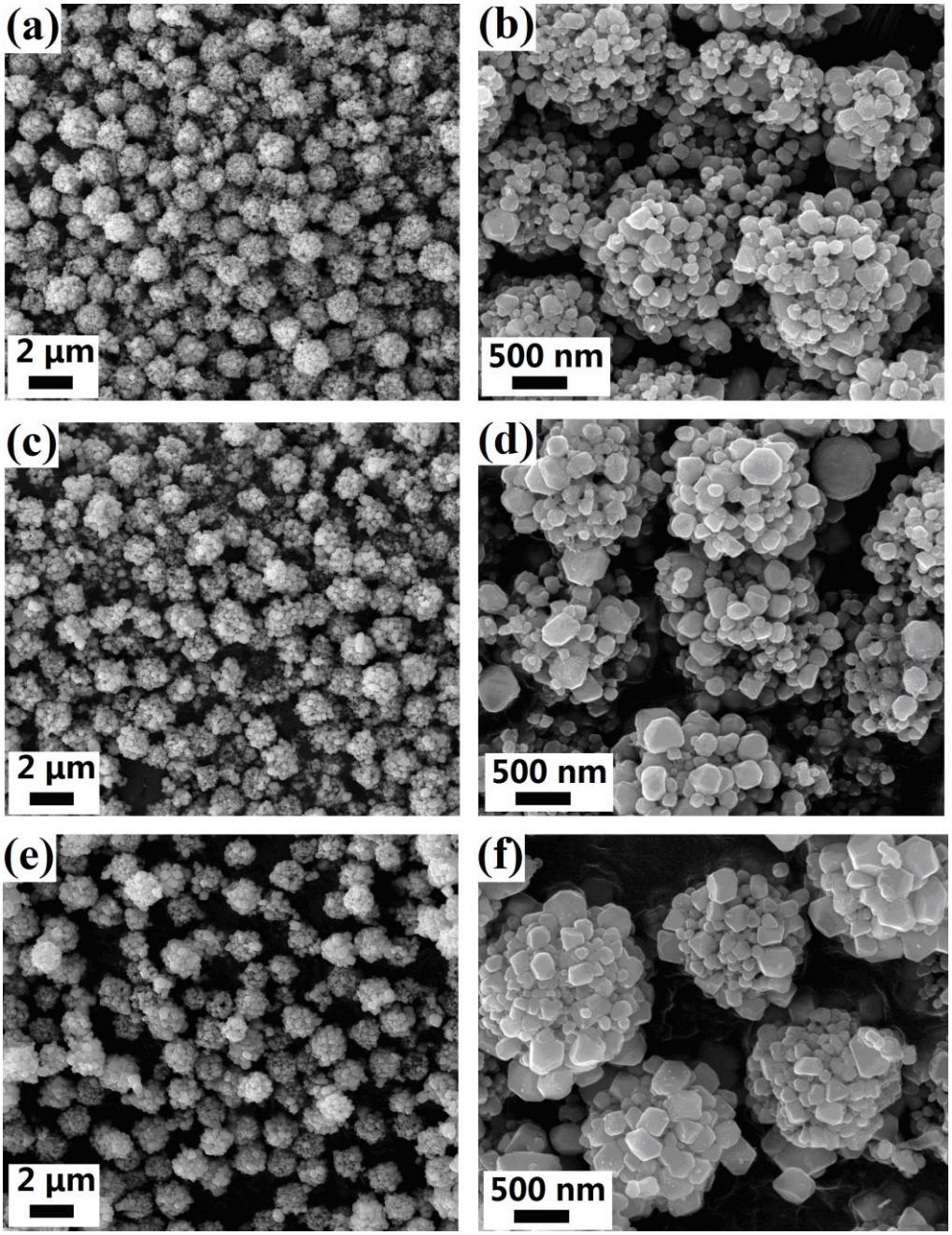

Figure S9 SEM images of hollow Cu particles with different shell thickness, synthesized by the etching of Cu@SiO_2. (a) and (b) 28 nm, (c) and (d) 45 nm, and (e) and (f) 60 nm.

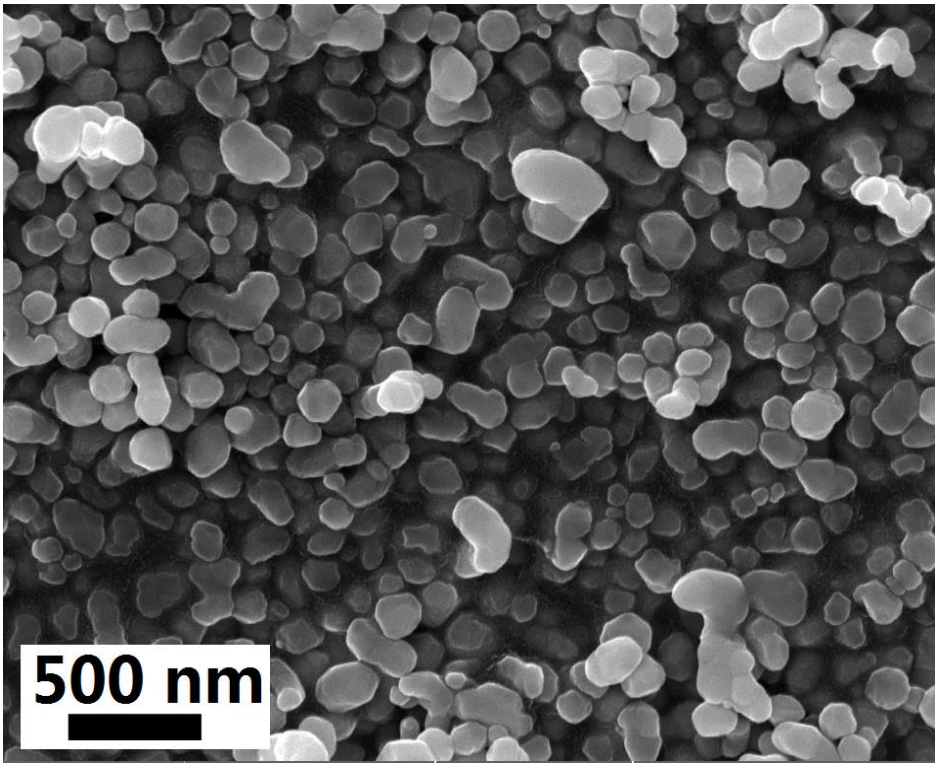

Figure S10 SEM image of particles from the PEG-400 reduction of Cu_2O NPAs at 240 °C

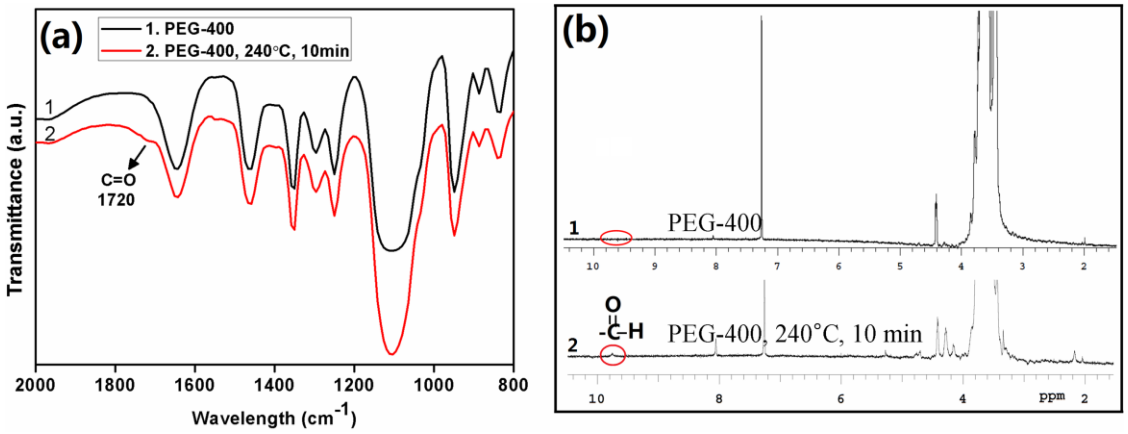

Figure S11 IR (a) and ^1H NMR (b) spectra of PEG-400 and PEG-400 solution under 240 °C for 10 min.

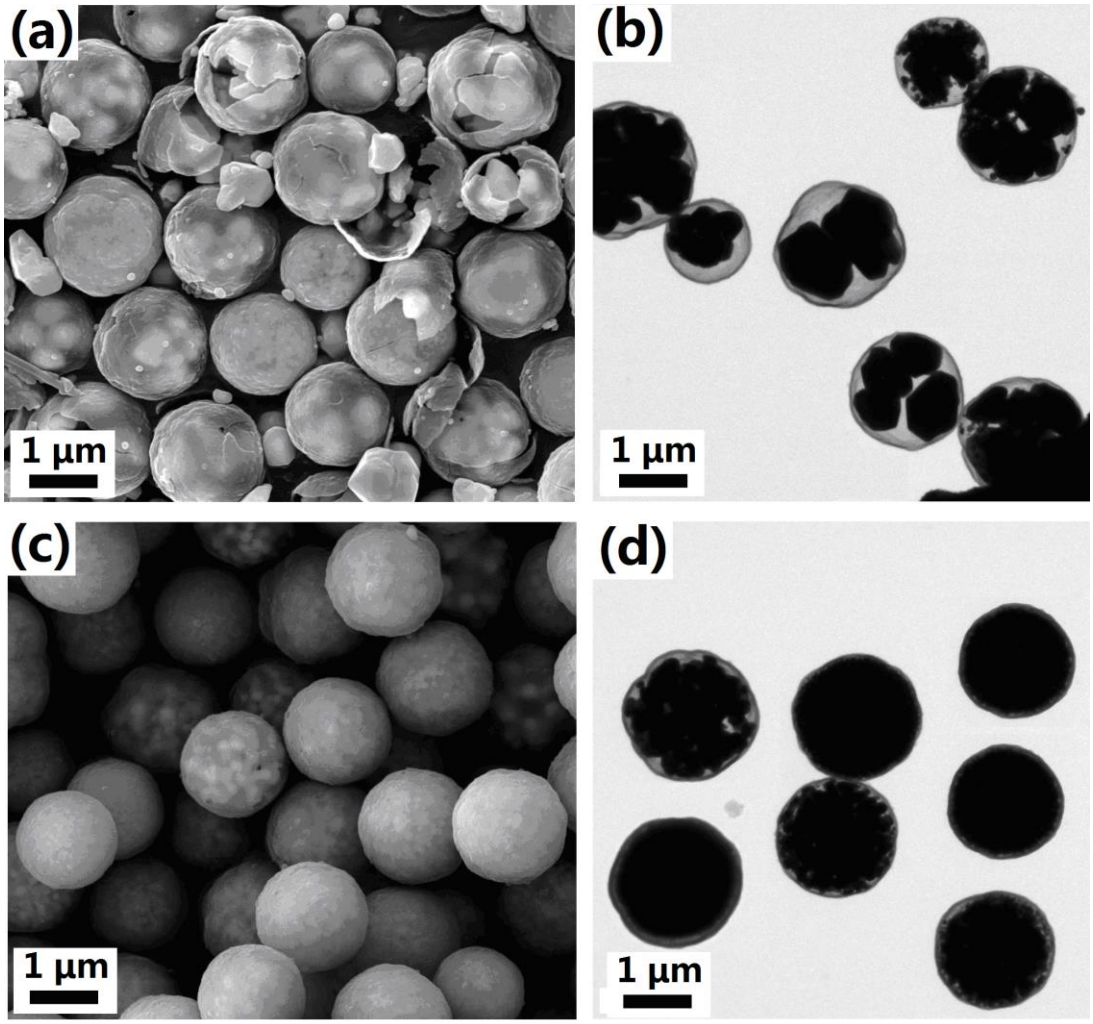

Figure S12 SEM images of particles with a shell thickness of 43 nm, synthesized from the reduction with glycerol (a) and PEG-10,000 (c). (b) and (d) are the relevant TEM images.

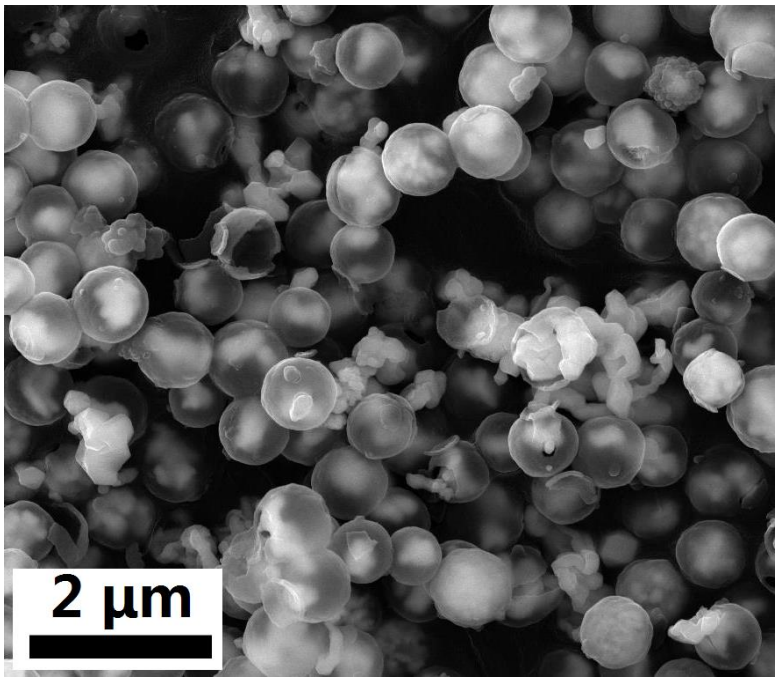

Figure S13 SEM image of particles with a shell thickness of 43 nm, from PEG-400 reduction under 270 °C.

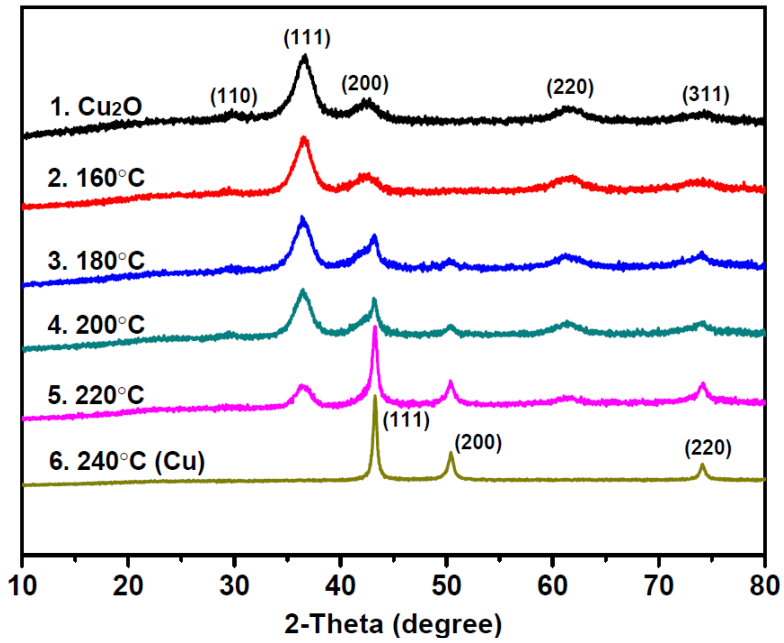

Figure S14 XRD patterns of particles from the PEG-400 reduction of Cu2O@SiO2 (43 nm) under different temperatures for 30 min.

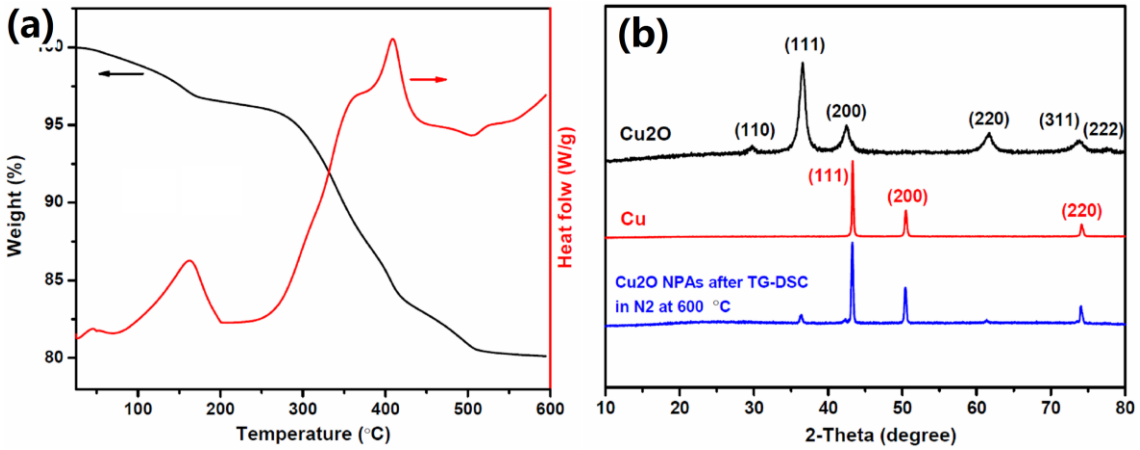

Figure S15 (a) DSC-TG measurement of Cu_2O NPAs in N_2 environment. (b) XRD patterns of samples.

Theoretically, the weight loss of $Cu_2O@SiO_2$ particles after reducing to $Cu@SiO_2$ is approximately 11%. According to the TGA curve, the weight loss of $Cu_2O@SiO_2$ particles is 20%. After DSC-TG measurement of Cu_2O NPAs in N_2, the XRD pattern revealed that it was dominated by the diffraction peaks of Cu. Thus, it is deduced that the PVP content is approximately 9 wt%.

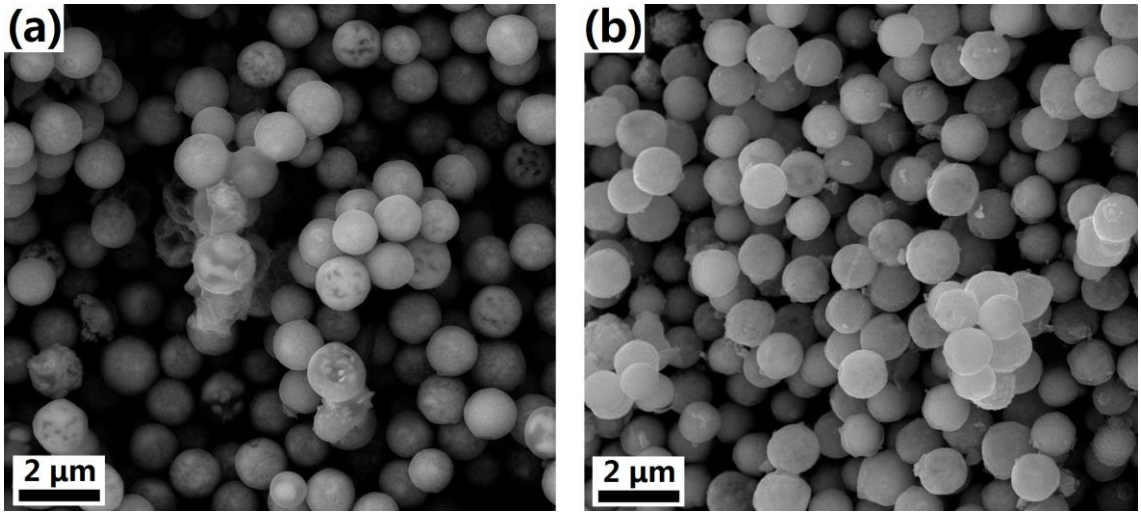

Figure S16 SEM images of particles sintered at 600 °C for 1 h (a) with a shell thickness of 88 nm, and (b) 45 nm.

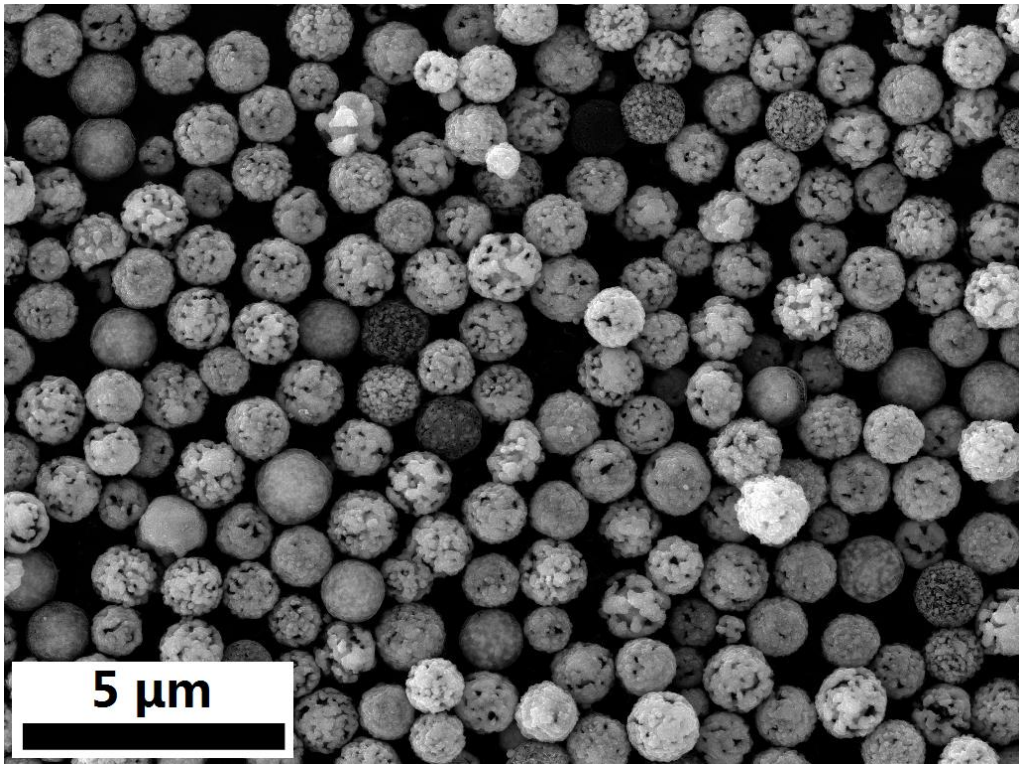

Figure S17 SEM image of hollow Cu particles with an average size of 1.5 µm.

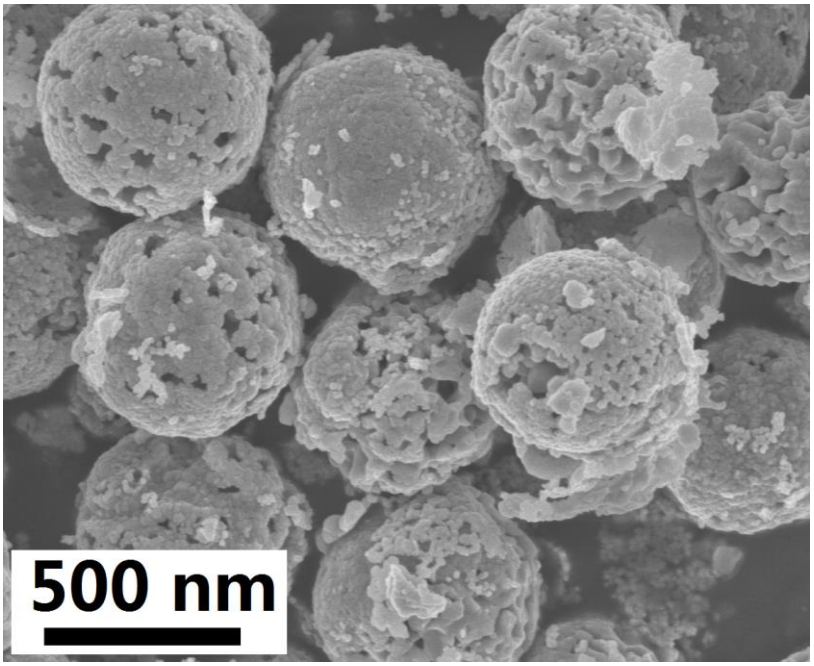

Figure S18 SEM image of hollow Cu particles with an average size of 500 nm.

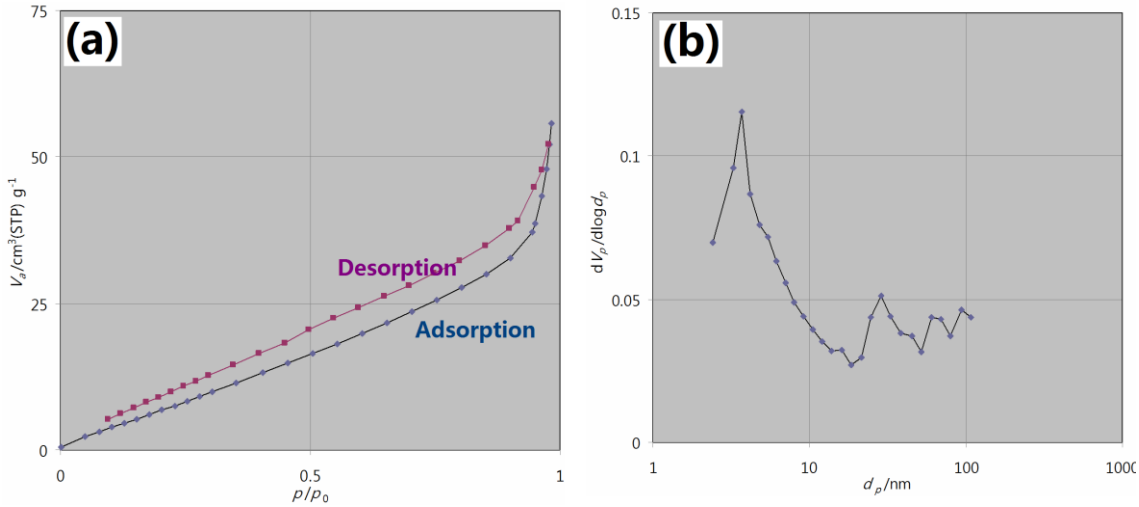

Figure S19 N_2 adsorption-desorption isotherms for hollow Cu particles (1.5 μm), with corresponding BJH pore-size distributions.

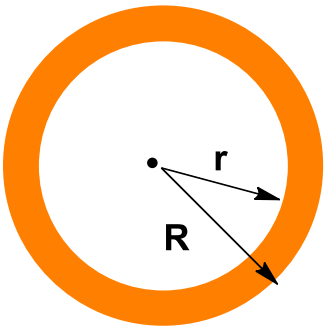

mass of hollow Cu (M): $\rho_{Cu} \times V_{Cu\ shell}$

$$\rho_{Cu} \times \frac{4}{3}\pi\,(R^3 - r^3)$$

Volume of hollow Cu (V): $\frac{4}{3}\pi R^3$

The density of hollow Cu: $\frac{M}{V} = \left[1 - \left(\frac{r}{R}\right)^3\right] \times \rho_{Cu}$

$$\frac{V_{Cu\ shell}}{V_{Cu2O}} = \frac{\frac{4}{3}\pi\,(R^3 - r^3)}{\frac{4}{3}\pi R^3} = 1 - \left(\frac{r}{R}\right)^3$$

Figure S20 Calculation of the density of hollow Cu particles

R and r are the average outer and inner radii of hollow particles, respectively. ρ_{Cu} is the density of solid Cu (8.96 g/cm^3).

Previously, our calculation revealed that the Cu_2O volume is reduced by 70% to form Cu powders, making a highly porous structure, i.e., the reduced Cu NPs occupy only 30% of the Cu_2O volume (V_{Cu2O}). Therefore, $V_{Cu\ shell}$ / V_{Cu2O} is equal to 0.3. Accordingly, the density of hollow Cu is 0.3×8.96 g/cm^3 = 2.7 g/cm^3.

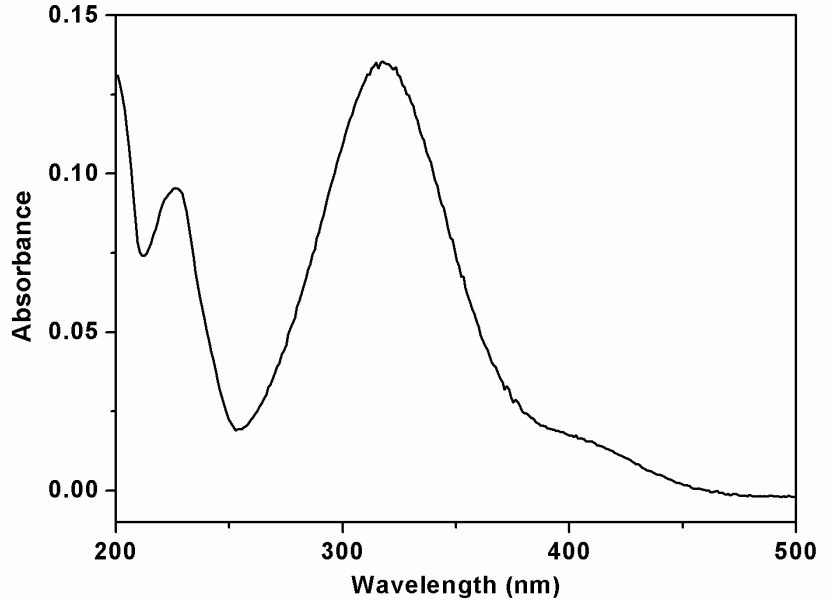

Figure S21 UV-vis spectrum of 4-NP in aqueous solution (12.5 μM).

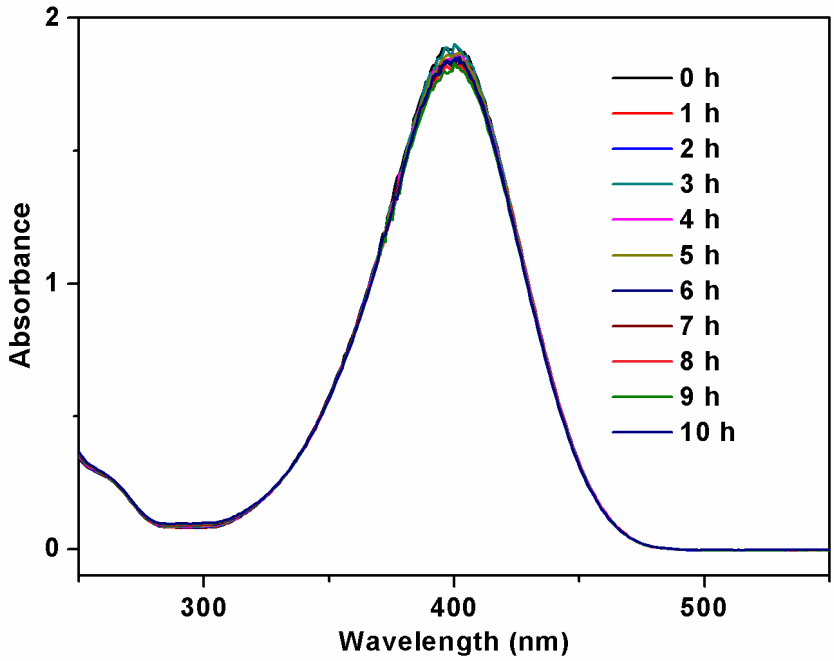

Figure S22 UV-vis spectra for the 4-NP reduction by NaBH4 at 25 °C without catalyst.

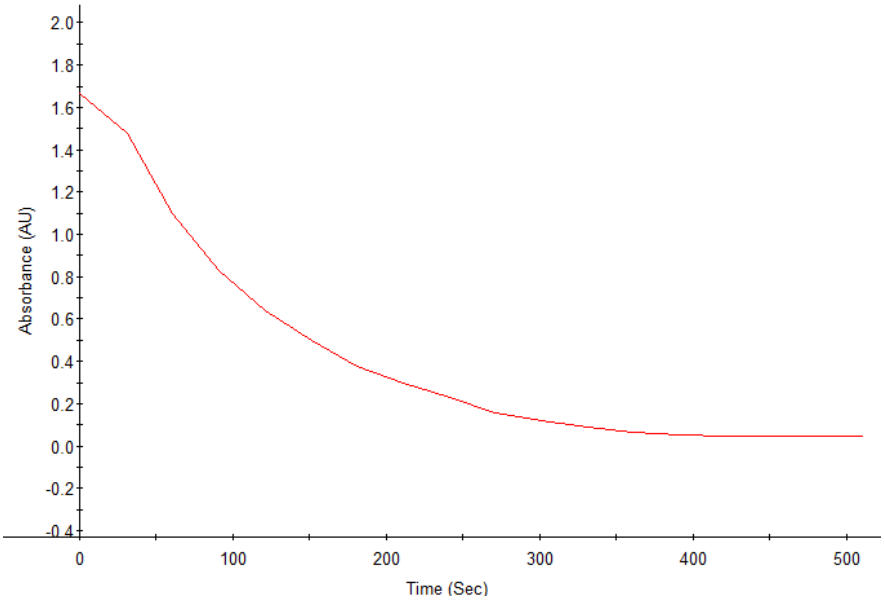

Figure S23 The absorbance versus time (*t*) plots for the reduction of 4-NP catalyzed by hollow porous Cu particles.

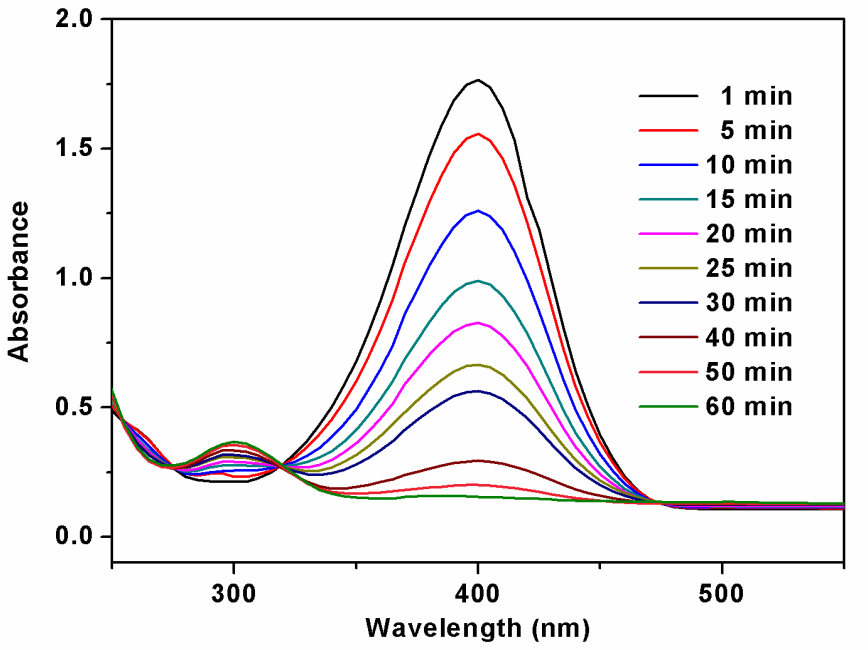

Figure S24 UV-vis spectra for the 4-NP reduction by $NaBH_4$ at 25 °C catalyzed by Cu NPs with an average size of 100 nm (0.02 mg/mL).

Table S1 Comparison of apparent rate constant (k_{app}) and activity factor (K) of different catalyst for the reduction of 4-NP.

Samples	Quality (μg)	k_{app} (s^{-1})	K ($s^{-1} g^{-1}$)	Reference
hollow porous Cu particles	50	0.0093	186	This work
Cu nanoplates	70	0.0095	136	S1
Cu 9.5 nm cubes	96	0.0101	105	S2
Cu 18.0 nm cubes	96	0.0057	60	S2
Cu 21.5 nm cubes	96	0.0041	43	S2
porous Cu microspheres	50	0.0041	82	S3
Cu nanobranches	50	0.0021	42	S3
solid Cu microspheres	50	0.0014	28	S3
porous Cu microspheres	60	0.0043	72	S4
porous Cu microspheres	500	0.0030	6	S5
In situ Cu NPs	12.5	0.0016	0.1	S6
Cu NPs	1000	0.0071	7.1	S7
Cu hydrosol 0.96 nm	58.2	0.0089	153	S8
Cu hydrosol 2.01 nm	58.2	0.0037	63	S8
Cu hydrosol 5.21 nm	58.2	0.0016	28	S8
Cu hydrosol 9.42 nm	58.2	0.0011	19	S8
Cu hydrosol 17.36 nm	58.2	0.0007	12	S8
Cu hydrosol 26.26 nm	58.2	0.0004	6	S8
Au/graphene hydrogel	24	0.0032	129	S9
Ag/SNTs-4	270	0.0384	142	S10
Pd/SPB-PS	38	0.0044	116	S11

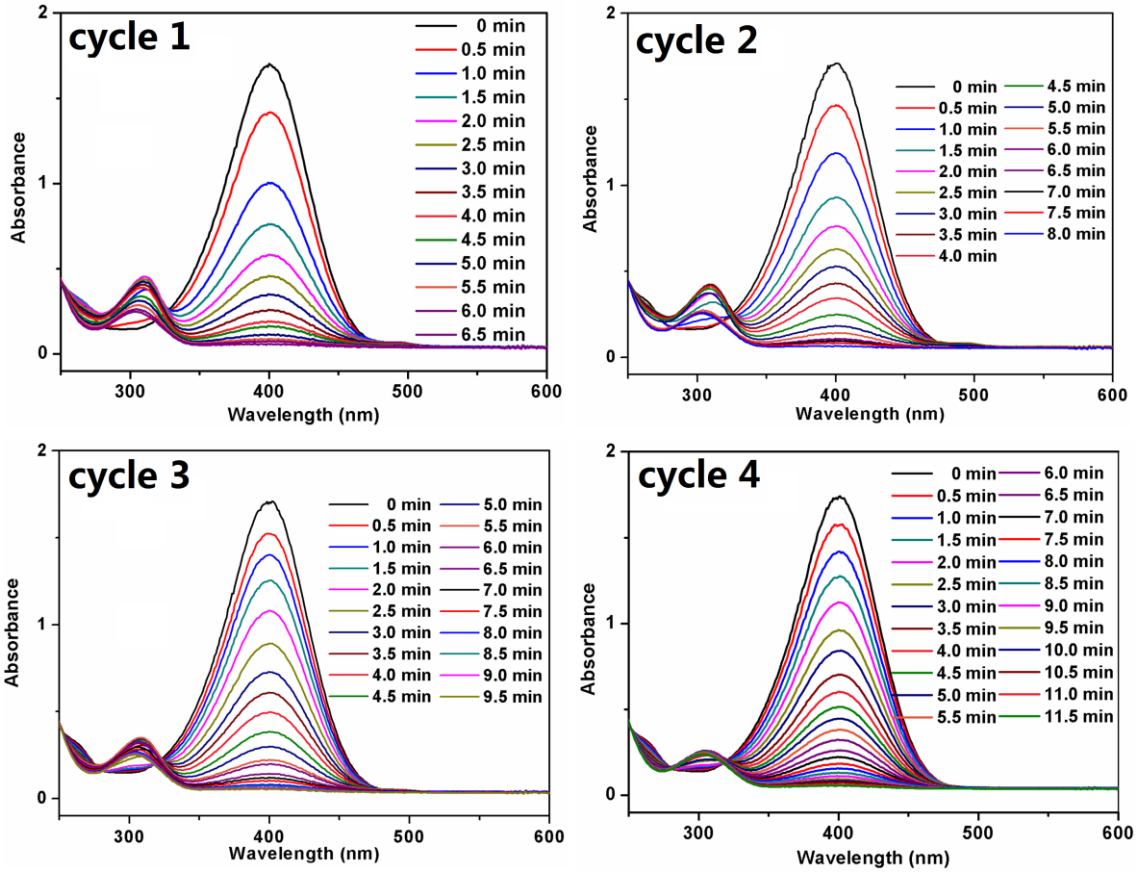

Figure S25 UV-vis spectra for the catalytic reduction of 4-NP with $NaBH_4$ in each cycle.

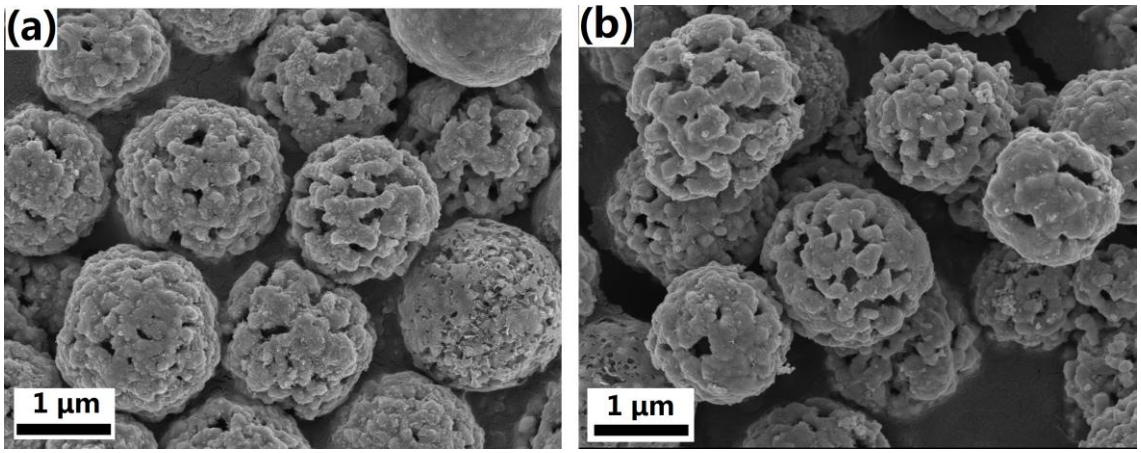

Figure S26 High-magnification of SEM images of hollow Cu particles before (a) and after (b) 4 cycles of reduction.

References in supporting information

S1 Y. Sun, L. Xu, Z. Yin and X. Song, *Journal of Materials Chemistry A*, 2013, **1,** 12361.

S2 P. Zhang, Y. Sui, G. Xiao, Y. Wang, C. Wang, B. Liu, G. Zou and B. Zou, *Journal of Materials Chemistry A*, 2013, **1,** 1632.

S3 M. Li, Y. Su, J. Hu, H. Geng, H. Wei, Z. Yang and Y. Zhang, *Materials Research Bulletin*, 2016, **83,** 329.

S4 S. Gao, X. Jia, J. Yang and X. Wei, *Journal of Materials Chemistry*, 2012, **22,** 21733.

S5 Y. Zhang, P. Zhu, L. Chen, G. Li, F. Zhou, D. Lu, R. Sun, F. Zhou and C.-p. Wong, *Journal of Materials Chemistry A*, 2014, **2,** 11966.

S6 P. Deka, R. C. Deka and P. Bharali, *New Journal of Chemistry*, 2014, **38,** 1789.

S7 A. K. Sasmal, S. Dutta and T. Pal, *Dalton Transactions*, 2016, **45,** 3139.

S8 Y. Zhang, P. Zhu, G. Li, W. Wang, L. Chen, D. D. Lu, R. Sun, F. Zhou and C. Wong, *Nanoscale*, 2015, **7,** 13775.

S9 J. Li, C.-y. Liu and Y. Liu, *Journal of Materials Chemistry*, 2012, **22,** 8426.

S10 Z. Zhang, C. Shao, Y. Sun, J. Mu, M. Zhang, P. Zhang, Z. Guo, P. Liang, C. Wang and Y. Liu, *Journal of Materials Chemistry*, 2012, **22,** 1387.

S11 Y. Mei, Y. Lu, F. Polzer, M. Ballauff and M. Drechsler, *Chemistry of Materials*, 2007, **19,** 1062.